Desalination and Water Treatment
www.deswater.com
doi: 10.5004/dwt.2020.24870

179 (2020) 312–322
March

Eriochrome Black T removal from water solution by modified $LaNiO_3$: kinetic, isotherm, and thermodynamic studies

Farhad Salimi[a,*], Sarie Pire[a], Changiz Karami[b]

[a]*Department of Chemical Engineering, Kermanshah Branch, Islamic Azad University, Kermanshah, Iran, emails: f.salimi@iauksh.ac.ir (F. Salimi), sariepire@yahoo.com (S. Pire)*
[b]*Nano Drug Delivery Research Center, Kermanshah University of Medical Sciences, Kermanshah, Iran, email: changiz.karami@gmail.com*

Received 15 March 2019; Accepted 8 September 2019

ABSTRACT

In this study, $LaNiO_3$ (LNO) and modified $LaNiO_3$ (MLNO) nanoparticles with perovskite structures were synthesized using the citrate sol–gel method and used for removal of the Eriochrome Black T (EBT) dye from water. The increase of the surface area on the LNO was created by enhancing the holes on its surface. The transmission electron microscopy, scanning electronic microscopy, the N_2 adsorption (Brunauer–Emmett–Teller specific surface area) and pore size distribution analysis and X-ray diffraction spectroscopy were used to characterize the prepared nanoparticles. The results of the surface area analysis indicated that the number of MLNO samples increased through the method applied in this paper. The effects of adsorbent dosage, pH, and contact time were investigated and 25.90 and 19.27 mg/g of LNO and MLNO were respectively obtained for the adsorption of the maximum EBT. The optimum conditions for 100 mg/L EBT solution were pH of 5 and 0.3 g/L LNO and MLNO. Freundlich isotherm and pseudo-second-order model better predicted the adsorption isotherm and adsorption kinetics, respectively. Moreover, thermodynamic parameters have been measured and results indicate that the adsorption process was spontaneous and exothermic for LNO and spontaneous and endothermic for MLNO.

Keywords: Adsorption; $LaNiO_3$ perovskite; Eriochrome Black T; Adsorption behavior; Thermodynamic parameters

1. Introduction

Annually, about one million tons of dyes are produced in the world, of which 70% in the market are azo dyes that are the largest class of the commercial dyes [1]. A reactive azo dye contains one or more azo bonds (–N=N–) that act as chromophores in the molecular structure [2]. Also, it is the largest group of organic dyes, which is challenging to degrade even at low concentrations due to its high resistance to light, heat, water, and chemical, and microbial attacks [3]. Therefore, it is highly essential to remove azo dyes from wastewater effluents before discharge into water bodies.

Today, the use of adsorbents have been increased to remove the dyes from wastewater [4–8]. A wide range of materials has been reported for dye removal, including zeolite, clay, activated carbon, and polymer. However, there are disadvantages associated with such materials. Thus, the development of new materials with good adsorption capacity, large surface area, and small diffusion resistance characteristics is still on demand [9]. Nanotechnology, as a novel method, offers a class of promising adsorbents that the shape of nanoparticles is essential because a wide range of the physical and chemical properties of these particles are entirely

* Corresponding author.

dependent on their sizes and morphologies. For example, optical or catalytic properties [10], CdTe tetrapods [11] and Cu_2O coated with Cu nanoparticles [12] depend on their morphologies are different.

Many techniques have been introduced to remove dyes from wastewaters. Biological, oxidation or ozonation [13,14], flocculation [15], membrane separation [16] and adsorption [17–19]. Among several abovementioned techniques for the removal of dyes from the water, adsorption methods are very efficient, economical, and widely in use for wastewater treatment [20]. Nanostructures, which are applied as novel materials for the removal of dyes, offer a class of promising adsorbents that are ultra-fine and have a large surface area.

The structure of perovskites (ABO_3) is the combination of rare earth elements (A) and transition metals (B). By changing these elements, a wide range of these structures can be synthesized. The rare-earth ion at the A-site supplies the thermal resistance of perovskites and the transition metal cation at the B-site attributes mainly to the catalytic activity. $LaNiO_3$ perovskite has been used for many targets such as electrode material and ferroelectrics because of its magnetic and conductive thin films [21]. The use of $LaNiO_3$ as a dyes removal in recent years has been of great interest to researchers [22], methane [23], and glycerol steam reforming to generate energy by producing a hydrogen-rich gas stream. The use of $LaNiO_3$ as a dyes removal in recent years has been of great interest to researchers [24,25]. These applications include the removable of methyl orange by $La_4Ni_3O_{10}$ [26], degradation of 4-chlorophenol in the presence of La_2NiO_4 [26], oxidation of phenol by using $LaBO_3$ (B: Cu, Fe, Mn, Co, Ni) [27], decolorization of Rhodamine B by $LaMO_3$ (M: Co, Cu, Fe and Ni) [28] and removal of reactive black dye by $LaNiO_3$ perovskite [29].

In continuation of our previous research on adsorption of dyes from aqueous solution [30–35]. The purpose of this research is the synthesis and characterization of LNO and LNO modified with $Zn(NO_3)_2$ and comparing adsorption of Eriochrome Black T (EBT) dyes in different parameters such as contact time, pH, and adsorbent dosage. Adsorption and kinetic isotherms and also thermodynamic models were considered to obtain the useful parameters to dye adsorption processes.

2. Materials and methods

Many materials including of Citric acid (99% $C_6H_8O_7$, Merck, Germany), ethylene glycol (99% ($C_2H_4(OH)_2$, Merck, Germany) nickel nitrate salt (99% (Ni $(NO_3)_2\cdot 6H_2O$, Merck, Germany), lanthanum nitrate salt (99% La $(NO_3)_2\cdot 6H_2O$, Merck, Germany), zinc nitrate salt (Zn $(NO_3)_2 6H_2O$, 99%, Merck) and ammonium chloride (NH_4Cl, 99%, Merck, Germany) were used. The EBT, high quality, was prepared by Merck Company.

2.1. Instruments

Perovskite-structure, particle size and phase purity of the samples were investigated by X-ray diffraction (XRD, PHILIPS PW 1840, k = 1.54056 Å). Typically, the peaks of the adsorbent diffraction pattern in the 2θ range between 10° and 80° were scan with a velocity of 1.5°min^{-1}. For measure nanoparticles size, a transmission electron microscopy (TEM) (PHILIPS CM200 FEG apparatus) and a scanning electron microscope (PHILIPS XL30) were used. A Cary 100 UV–visible spectrometer (Varian, USA) was used to study UV–visible absorption spectra at 23°C–25°C temperature. To determine the nickel, lanthanum metals and zinc content in the structure, the atomic absorption (AA) spectroscopy (AAS-009 model) and inductively coupled plasma (ICP) emission spectroscopy (Perkin-Elmer ICP/5500) were used. The Brunauer–Emmett–Teller (BET) method (Quantachrome CHEMBET-300) was used for evaluating the surface area.

2.2. Synthesis of LNO and MLNO perovskite structures

For synthesizing the LNO compound, first, 2 g of nickel nitrate was added to a mixture of the citric acid (10.51 g) and ethylene glycol (3.41 g) in 50 mL distilled water under vigorous stirring. The molar ratio of citric acid to nickel nitrate was 5, and it was 1 for ethylene glycol to citric acid. After the nickel nitrate is completely dissolved, the lanthanum nitrate (3.55 g) was added to the stoichiometric ratio. The solution was obtained at 60°C until a gel with high viscosity was mixed slowly by a magnetic stirrer for 12–24 h. The obtained gel for calcination was placed in an electric furnace at a temperature of 800°C for 4 h. The heating rate was 1°C min^{-1} up to 400 and 3°C min^{-1} up to 800°C [36,37]. The structure of the perovskite (MLNO) is based on the previous method [38]. In this method, Zinc nitrate was used to make holes on the perovskite $LaNiO_3$ surface. In this experiment, the added Zn $(NO_3)_2$ in the final solution was transformed to ZnO with a perovskite structure. Next, the ammonium chloride (2 M concentration) was added to dissolve and exit ZnO from the perovskite structure. Afterward, the etching of this structure was done for 2 h with deionized water. After drying to stabilize the structure, the precipitate was re-calcined at 800°C. During the etching process, a small amount of ammonia is produced according to Eq. (1).

$$2NH_4Cl + ZnO \rightarrow 2NH_3 + ZnCl_2 + H_2O \quad (1)$$

The reason behind the use of ZnO is the high ion radius and the formation of a hole in the perovskite structure, and also easy to dissolve and separate it after calcination of ZnO.

2.3. Method

For the study, the adsorption ability of EBT dye, several parameters are investigated, which include pH, adsorbent dosage, temperature and time. For adsorption experiments, the amount of 0.003–0.02 g of adsorbent was mixed with 10 ml of EBT dye solution to a suitable concentration and pH after shaking 200 rpm and constant temperature. The pH value was adjusted between 2 to 12 using HCl (0.1 mol/L) or NaOH (0.1 mol/L) solution. Finally, using the spectrophotometer and the following equation were measured the amount of adsorption.

$$\%\text{Removal} = \frac{\left(C_i - C_f\right)}{C_i} \times 100 \quad (2)$$

C_f is the initial and the C_i final concentrations of EBT in solution. The following equivalent is then used to measure the adsorption capacity:

$$q_e = \frac{\left(C_0 - C_e\right)V}{M} \tag{3}$$

In this equation, the q_e is the amount of adsorption capacity, and the C_e and C_0, respectively, indicate a balanced and initial concentration of dye in solution (mg/L). Other parameters that are seen in the equation are V and M which indicate the solution volume (L) and dosage of the adsorbent (g), respectively [39].

2.4. Point of zero charge determination

The point of zero charge (PZC) was calculated using the following method: to completely remove the CO_2 dissolved in the water, 100 ml of deionized water added to an Erlenmeyer flask which capped with cotton and then heated for 20 min. Then 10 mL of it was added to a 25 mL Erlenmeyer flask with 0.5 g of adsorbent and mix it for 48 h at 25°C. Finally; the solution pH indicates the PZC. This method has been used satisfactorily [40–42].

2.5. Adsorption isotherms

Langmuir and Freundlich are two more common isotherms that widely used to describe the adsorption processes. The Langmuir isotherm model is the first isotherm adsorption, which is based on the molecules, or ions, bond to certain points at the surface of the adsorbent material, and monolayer adsorption occurs. Also, no interaction occurs between adsorbed molecules [43]. This equation has been derived from Gibbs' method which has been shown in Eq. (3).

$$\frac{C_e}{q_e} = \frac{C_e}{q_{\max}} + \frac{1}{bq_{\max}} \tag{4}$$

In which, b (L/g) is the Langmuir constant that is related to the free energy of adsorption, $q_{\max}$ (mg/g) is the monolayer adsorption capacity, C_e (mg/L) is the adsorbate equilibrium concentration in solution and q_e (mg/g) is the concentration of adsorbate on the surface of adsorber.

A dimensionless constant, R_L, known as separation factor, can be used to explain the essential characteristics of Langmuir isotherm, which is calculated using the following equation.

$$R_L = \frac{1}{\left(1 + bC_0\right)} \tag{5}$$

where b is the Langmuir adsorption constant (L mg^{-1}) and C_0 (mg L^{-1}) is the initial liquid phase concentration of an analyte. The value of R_L explicates the adsorption process to be linear ($R_L = 1$), unfavorable ($R_L > 1$), favorable ($0 < R_L < 1$), or irreversible ($R_L = 0$) [44].

The basis of the equilibrium Freundlich isotherm is the adsorption occurs at a heterogeneous surface that energy is not distributed uniformly. This heterogeneity leads to the creation of various functional groups on the adsorbent and, consequently, promotes the formation of various mechanisms at an interaction between adsorbent and adsorbent [45]. This model is displayed as follow:

$$q_e = K_F C_e^{\frac{1}{n}} \tag{6}$$

where q_e (mg g^{-1}) is the dose of dye adsorbed on the surface (mg g^{-1}), K_F is an estimated indicator of adsorption capacity. The adsorption process is favorable for $1/n$ between 0 and 1, it is difficult to carry out If $1/n \geq 2$.

2.6. Kinetics studies

To study the kinetic adsorption of adsorbents and dye, the equations of pseudo-first and the pseudo-second was used. In the equations of the pseudo-first equation, the intensity of adsorbent sites filling is proportional to some vacant sites and driving forces are considered to be linear. The pseudo-second equation is based on the level of equilibrium capacity, in which the intensity of adsorbent sites filling is found to be proportional to the square of the number of vacant sites of the adsorbent. The linear form of the pseudo-first and pseudo-second kinetic equations is shown in the following equations [46,47]:

$$\ln\left(q_e - q_t\right) = \ln\left(q_e\right) - k_1 t \tag{7}$$

$$\frac{t}{q_t} = \frac{1}{k_2\left(q_e\right)^2} + \frac{t}{q_e} \tag{8}$$

q_t and q_e are the amount adsorption capacities (mg/g) and t is the time (min) at the equilibrium, and k_1 and k_2, respectively, are the first and second rate constant (L/min).

3. Results and discussion

3.1. Analysis of scanning electronic microscopy and TEM

The images of scanning electronic microscopy (SEM) and TEM related to the LNO and MLNO are shown in Fig. 1. From the SEM image of two structures, it can be concluded that the nanosized structure is spherical particles. The results from the TEM images are shown that the diameter of the particles is 20–40 nm and the TEM image of the MLNO is also spherical with 20–40 nm in diameter. However, the size of these particles is in the range of the nanoscale.

The findings of the XRD test for two samples of LNO and MLNO are presented in Fig. 2. Compared to standard cards, nanoparticles, or nano-adsorbents, are well-synthesis because the sample peaks are similar to the standard sample $LaNiO_3$ (reference code: 0633-088-01). And also results show that the LNO structure has a perovskite crystal phase without any other crystalline phases by a relatively sharp peak [48,49]. The particle diameter (i.e., 31 nm) was calculated using the Scherer equation for a high peak at 2θ = 47.3°. As mentioned before, to increase the $LaNiO_3$ surface area, etching operations using zinc nitrate were performed. XRD

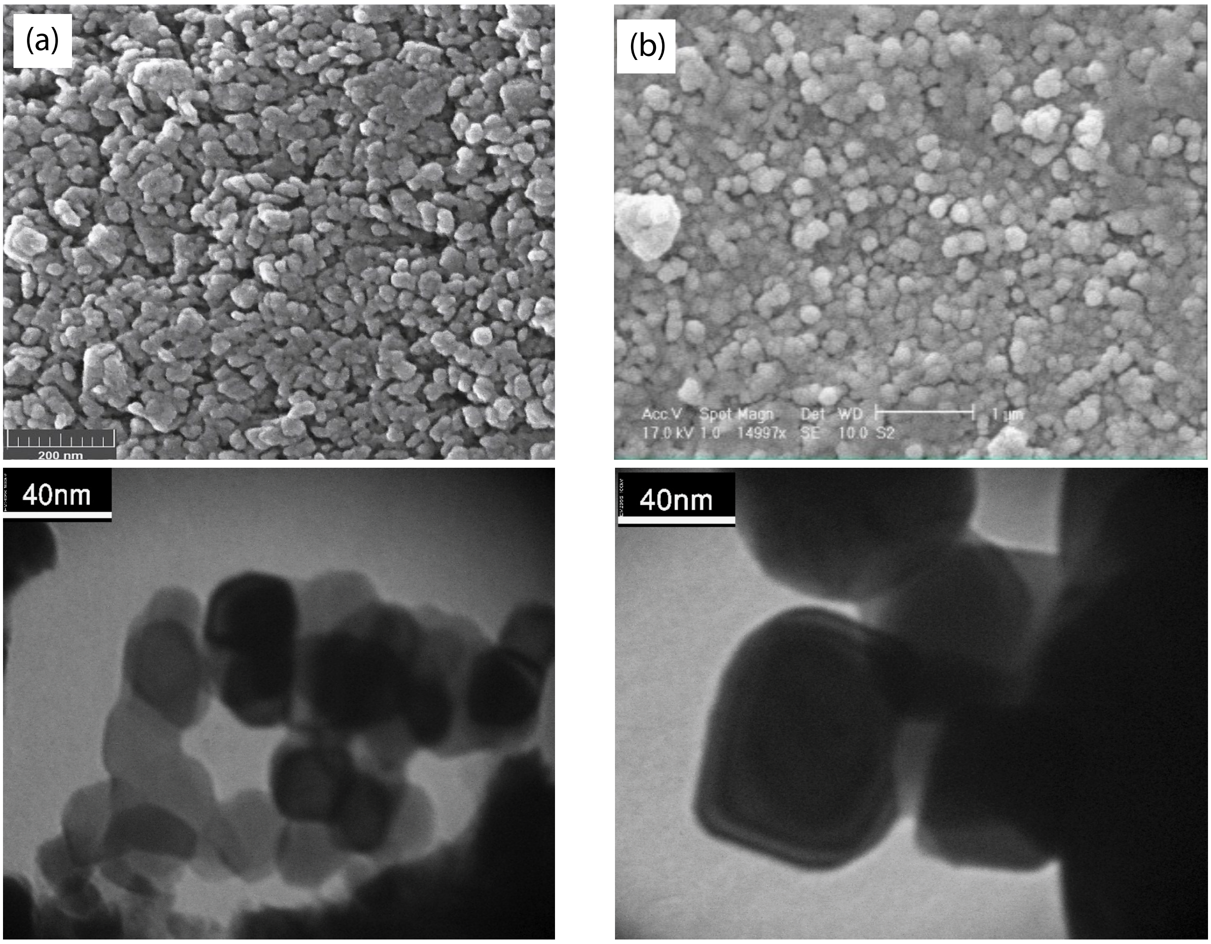

Fig. 1. SEM and TEM images of (a) LNO and (b) MLNO perovskite surface.

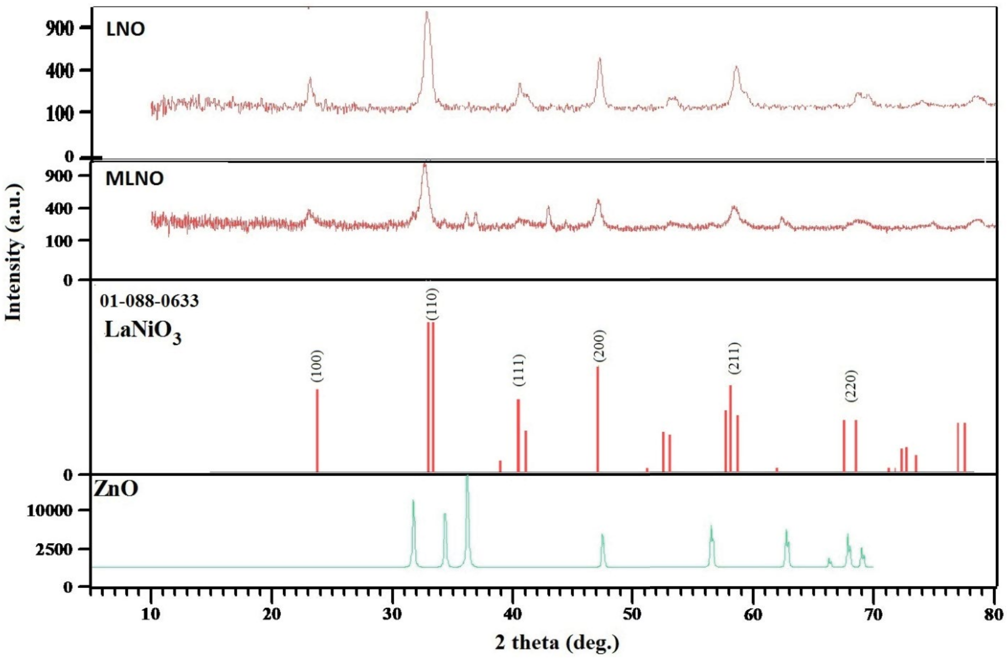

Fig. 2. Real and referenced XRD patterns of LNO and MLNO samples after calcination at 800°C (JCPDS# 33-0710).

patterns of the $LaNiO_3$ after etching are shown in Fig. 2. After the etching operation, given that the original structure of $LaNiO_3$ is retained, a small amount of zinc oxide is also present in the XRD spectrum.

3.2. BET, ICP, and AA analysis

Table 1 shows the results of the analysis of the ICP and the surface area by the BET method of the $LaNiO_3$ perovskite catalyst.

The results of ICP showed that the weight percentage of Ni in the MLNO was decreased due to the presence of the ZnO compound in the etching process. The special surface in the structure of LNO is less than that of the MLNO structure, which is synthesized by the sol-gel citrate method [38]. It can be stated that the specific surface for the composition of MLNO is three times higher than LNO. This result is attributed to the presence of zinc oxide with a diameter of 0.75 Å, which was created in the etching process in the final structure of MLNO and increased active surfaces [38]. The results obtained from the study of the active surface in the perovskite structure (LNO) show that the active surface is low, which is due to the synthesis of this structure with the high-temperature sol–gel citrate method and It is consistent with the results presented by other researchers [50]. In the structure of MLNO, Zn has an effective atomic radius of 0.75 Å, which has an active surface of about three times that of LNO. The replacement of the zinc element prior to acidification instead of the nickel element with an effective atomic radius of 0.6 Å provides a cavity in the final structure of MLNO and contains a field for increasing the surface activity of the sample [38]. However, this structure was synthesized with a much higher active surface (30 m^2/g).

3.3. Studying the pH effect on the removal efficiency

One of the key factors in the general adsorption process is the effect of pH, which affects the chemical properties of both materials adsorbents and dyes in solution. To study the effect of pH on the adsorption process, 0.005 g of adsorbent added to 10 mL, 100 ppm of EBT solution and the pH of the solution was set at 2–11. Fig. 3 clearly shows the dependence of pH on the EBT adsorption efficiency onto the adsorbents. For the LNO and MLNO adsorbents, with increasing the pH value, from pH 2 to 5, the dye removal is maximum and when the pH value > 5, the removal amount of EBT was decreased to a minimum level. Thus, pH = 5 was selected as the best pH. At lower pH values ($pH < pH_{PZC}$), the adsorbent had a positive charge. Moreover, EBT may be present in anionic forms. In such conditions, EBT molecules have a high tendency with it. By increasing the pH value ($pH \geq pH_{PZC}$), it tends to change in inverse [51]. The PZC of the LNO and MLNO are 8.3 and 7.7, respectively, the adsorbent surface is positive charge in $pH < pH_{PZC}$, then the dye contains negative charge will combine with adsorbent easily [52,53].

To examine the effect of the adsorbent dosage on the dye removal, different dosages of the adsorbent for adsorption of the 100 ppm EBT solution were used. Results in Fig. 4 show that by increasing the adsorbent dosage of LNO from 0.003 to 0.03 g led to a decrease in the dye removal rate. The obtained optimal mass for the LNO adsorbent was equal to 0.003 g. Similar results were obtained for MLNO, with a bigger rate of decline, where the optimal mass for the adsorbent was measured as 0.003 g. Results showed that the adsorption capacity is decreased with increasing adsorbent dosage, which may be attributed to adsorption sites saturation on an adsorbent surface due to particulate interaction such as aggregation, which would lead to a decrease in total surface area of the adsorbent [54].

Table 1
Elemental analysis (by ICP and AA tests), and BET surface areas of $LaNiO_3$ sample before and after etching

	LNO	MLNO
La (%)	67.5	68.8
Ni (%)	32.5	26.4
Zn (%)	–	4.5
Surface area (m^2/g)	3.15	8.6
Mean pore diameter (nm)	25.2	14.3

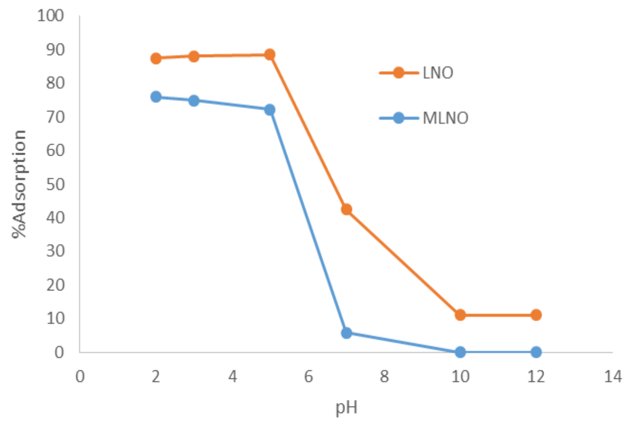

Fig. 3. Effect of pH on adsorption EBT dye on the adsorbents (conditions: 5 mg adsorbent, 10 ml of 100 mg/L of dye, duration of oscillation time of 30 min).

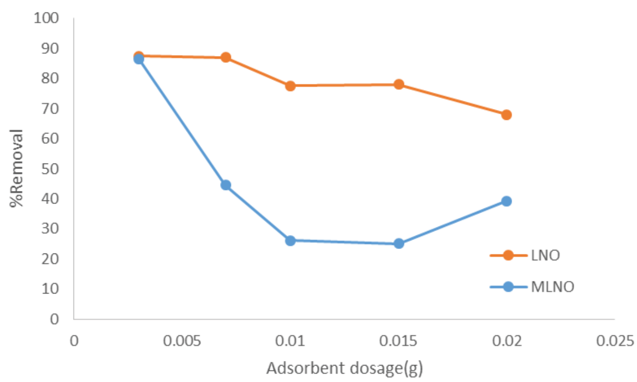

Fig. 4 Effect of adsorbent dosage on adsorption of dye on the adsorbents (conditions: 10 ml of 100 mg/L of EBT, duration of oscillation time of 30 min).

The results in Fig. 5 show that the removal efficiency increases by 88% of the removal dye with an increase in the contact time until 20 min. However, as time increased, EBT removal decreased because the availability and abundance of empty sites on the surface of the adsorbent were lower. As a result, the highest dye removal occurred in the first few minutes.

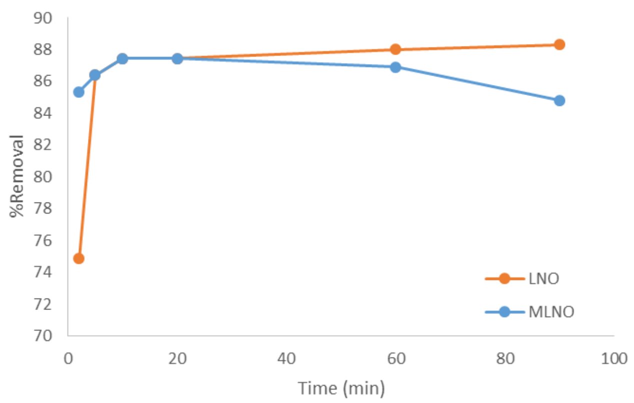

Fig. 5. Effect of reaction time on adsorption of EBT on the adsorbents (conditions: 10 ml of 100 mg/L of EBT).

3.4. Results of the adsorption isotherms and kinetics

Fig. 6 presents the adsorption isotherm of adsorbents for EBT dye which was fitted based on the adsorption process data. Table 2 presents the correlation coefficients and the adsorbent parameters. As shown in Table 2, the Freundlich model well fitted the adsorption isotherms, and theoretically, capacity adsorption has the highest amount.

The EBT dye adsorption on the adsorbents carries out quickly, as is inferred from the values of $1/n$ and R_L values obtained from the Langmuir and Freundlich models, respectively, however, the adsorption of dye carries out favorable. By considering the results of this section that we can conclude that there is multilayer adsorption for the EBT dye on the adsorbents.

Kinetic models can be used as an appropriate model that has information for understanding the adsorption mechanisms. The most widely used equations are the pseudo-first and second-order models. These two models were used to studying the adsorption kinetics of the EBT dye by adsorbents.

According to Fig. 7, the pseudo-second-order model was fitted best to the experimental data which indicates that the rate-limiting step is the chemical adsorption that involves electron transfer between the adsorbent and adsorbate by the

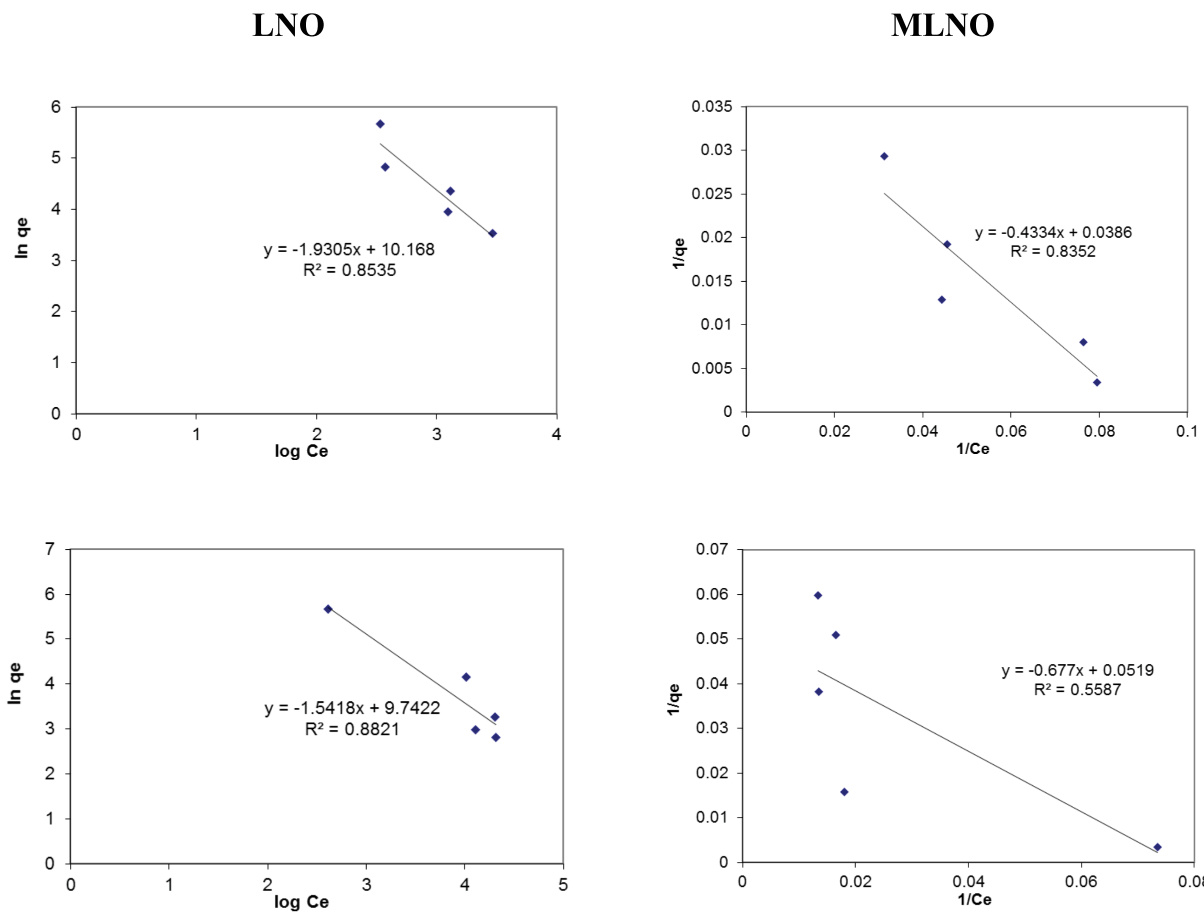

Fig. 6. Adsorption isotherms of dye adsorbed onto LNO and MLNO in aqueous solution; Langmuir model and Freundlich model.

Table 2
Comparison of dyes adsorption capacity of different adsorbents

Adsorption isotherm		MLNO	LNO
Langmuir equation	R^2	**0.5587**	**0.835**
	q_{max} (mg g^{-1})	**19.27**	**25.90**
	K_L (L mg^{-1})	0.0766	0.089
	R_L	0.115	0.102
Freundlich equation	R^2	**0.8821**	**0.854**
	K_F (mg g^{-1})	16,983	25,848
	$1/n$	0.649	0.518

valence force. The results of kinetic models are presented in Table 3.

3.5. Adsorption mechanism research

The pore size and pore volume are important properties considered in the manufacture of materials as adsorbents for specific applications. They are accessible to a molecule of a given size. The physical adsorption mechanism in small pore size is mainly pore filling because of the pore overlapping; thus, larger molecules cannot access the small pore size of the adsorbent. Table 2 shows the maximum adsorption capacities of the LNO is more than that of MLNO. These results also show that modifying the adsorbent increases surface area and pore volume but does not lead to an enhancement in dye adsorption. It seems that the narrowing the pore size in the MLNO leads to an increase in the steric hindrance of the EBT molecules on the adsorbent surface and reduces the amount of adsorption. The results show that modification of the adsorbent surface, which increases the specific surface area and adsorbent porosity, does not increase dye adsorption. Shrinking the size of the cavities in the MLNO has caused the steric effects of the EBT dye to increase the adsorbent surface and reduced the amount of adsorption of the dye.

3.6. Thermodynamic studies

The changes of enthalpy ($\Delta H°$), Gibb's free energy ($\Delta G°$) and entropy ($\Delta S°$) for the adsorption were determined by:

$$\ln K_L = \frac{\Delta S°}{R} - \frac{\Delta H°}{RT} \quad (9)$$

$$\Delta G° = \Delta H° - T\Delta S° \quad (10)$$

where R is the universal gas constant (8.314 J K^{-1} mol^{-1}), T is the solution temperature (K) and K_L is the equilibrium constant [55]. The calculated parameters of thermodynamic are demonstrated in Table 4.

The values of Gibbs free energy $\Delta G°$ had been calculated by knowing the $\Delta H°$ and the $\Delta S°$ and $\Delta H°$ was obtained from

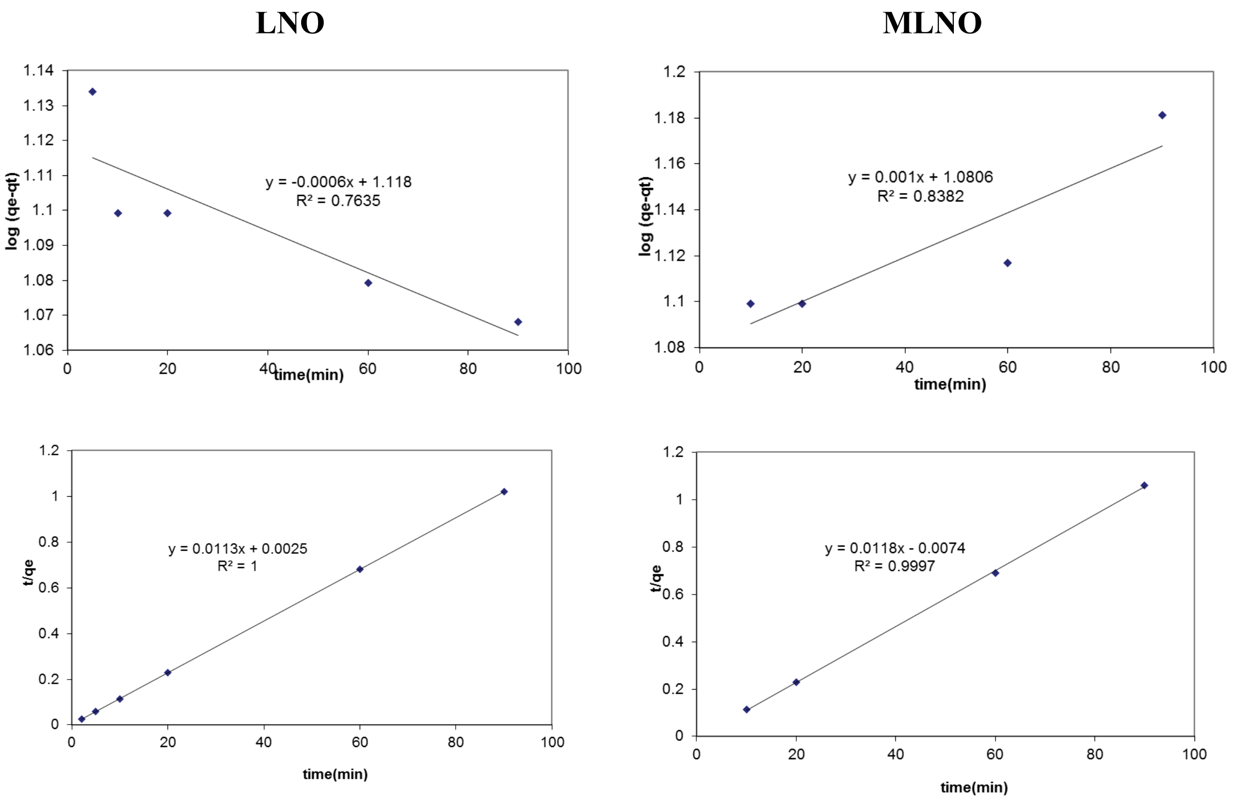

Fig. 7. Kinetic models for the adsorption of dyes; pseudo-first-order and pseudo-second-order kinetics.

Table 3
Pseudo-first-order model and pseudo-second-order model parameters constants for the adsorption of dyes on LNO and MLNO

	Pseudo-first-order model			Pseudo-second-order model		
Absorbents	k_1 (min^{-1})	q_e (mg g^{-1})	R^2	q_e (mg g^{-1})	k_2 (g mg^{-1} min^{-1})	R^2
MLNO	0.001	12.02	0.838	74.75	0.0188	0.9997
LNO	0.0006	13.12	0.763	88.49	0.0113	1

Table 4
Thermodynamic parameters for the adsorption of adsorbents at different temperatures

			$\Delta G°$ (kJ/mol)		
			T (°C)		
	$\Delta S°$ (kJ/mol)	$\Delta H°$ (kJ/mol)	20	35	50
MLNO	0.0134	2.2798	1.651	1.919	2.12
LNO	0.0386	–55.640	16.944	17.716	18.295

Table 5
Literature review on catalytic adsorption of dyes in the presence of various catalysts

Reference		Wang et al. [60]	Zou et al. [63]	Hua et al. [61]	Ovejero et al. [62]	Xu et al. [64]	Palas et al. [29]	This work	
Catalyst type		MoO_3	$La_{0.8}K_{0.2}FeO_3$	CuO/γ-Al_2O_3	Ni/MgAlO	Mo–Zn–Al, –O	$LaNiO_3$	$LaNiO_3$	Modified $LaNiO_3$
Dye		Rhodamine B	Methyl Blue	Methyl Orange, Direct Brown, Direct Green 1000	Basic Yellow 11	Cationic Red GTL	Reactive Black 5	EBT	EBT
Operating condition	Initial dye concentration, mg/L	5	500	1,000	200	85	100	100	100
	Catalyst loading, g/L	0.5	1	27.71	4	2.72	1	0.3	0.3
	Temperature, °C	Room temperature	20–50	80	100	Room temperature	50	Room temperature	Room temperature
	pH	–	–	3	–	4	3	5	5
	Time, min	180	30	120	180	60	120	20	20
Dye removal efficiency		85.9%	~80%	99%	83%	80.1%	65.4%	88%	88%

the plot of lnK_L vs. 1/T, from Eq. (8). Once these two parameters were obtained, ΔG° was determined from Eq. (9). The increased randomness at the solid/solution interface during the adsorption happens when the value of ΔS° is positive [56,57]. The negative values of ΔG° in Table 4 reveal that EBT dye adsorption by adsorbents is spontaneous processes. Also, it is considered that the ΔG° values decreased with temperature growth from 20°C to 60°C, indicating that the method was more efficient at the higher temperature. Furthermore, the values of ΔG° of less than −15 kJ mol^{-1} for unmodified adsorbent show that the interactions between dye molecules and adsorbent sites are physical. Moreover, according to the Table 4 for dye adsorption by adsorbents, the positive amount of ΔS° and negative value of ΔH° represents that the process is exothermic with increasing in randomness at the solid-solution interface within adsorption [58]. The lower adsorption heat obtained for modified adsorbent indicated that physical rather than the chemisorption adsorption was prevailing [59]. The endothermic process happens when the value of ΔH is positive, which means that the reaction consumes energy.

3.7. Compare this research with previous research

Table 5 shows a comparison between previous research works that have various transition metal-containing with this research [29,60–63]. The dye removal efficiencies using perovskite structure is rarely reported in the literature such that no study is available on EBT removal in the presence of $LaNiO_3$ structure.

In various studies (Table 5), the initial concentration of dye is between 5 and 1,000 mg/L. While in this research, 0.3 g/L of $LaNiO_3$ removal the amount of 100 mg/L dye solution. Since highly concentrated dye solutions dye is more difficult to remove. For instance, 27.71 g/L of CuO/g-Al_2O_3 for the treatment of 1,000 mg/L and 4 g/L of Ni/MgAlO used for the treatment of 200 mg/L 27.71 g/L of CuO/g-Al_2O_3 for the treatment of 1,000 mg/L dye solutions [61,62].

To evaluate the practical applications of a system for removing the dye, the reaction time is a very important parameter. In this regard, different times have been investigated for up to 180 min. Reviewing the past papers, it can be concluded that the $LaNiO_3$ structure has a high power of dyes removal at a better time.

4. Conclusion

In this study, the ability of EBT removal from aqueous solutions was examined by modified $LaNiO_3$ nanoparticles. Identification of the structure of the fabricated adsorbent was done using XRD, SEM, TEM, and BET. To obtain the optimized conditions for studying the efficiency of $LaNiO_3$ structure (as a compound for dye removal), parameters such as gram content of $LaNiO_3$, reaction time, pH of the solution, and initial concentration of EBT dye were studied. The results of the present study can be outlined as follows:

- The optimum conditions for 100 mg/L EBT solution were pH of 5 and 0.3 g/L $LaNiO_3$ and modified $LaNiO_3$.
- With increasing the dosage of MLNO, the adsorption amount decreased.
- Freundlich isotherm and pseudo-second-order model better predicted the adsorption kinetics and adsorption kinetics, respectively.
- The measuring thermodynamic parameters showed that the adsorption process was spontaneous and exothermic in nature for LNO and spontaneous and endothermic for MLNO.

The results show that the structure of $LaNiO_3$ perovskite has high efficiency for dye of EBT removal from industrial wastewater treatment.

References

[1] M. Stoyanova, I. Slavova, S. Christoskova, V. Ivanova, Catalytic performance of supported nanosized cobalt and iron–cobalt mixed oxides on MgO in oxidative degradation of Acid Orange 7 azo dye with peroxymonosulfate, Appl. Catal., A, 476 (2014) 121–132.
[2] A. Ahmad, B. Hameed, Fixed-bed adsorption of reactive azo dye onto granular activated carbon prepared from waste, J. Hazard. Mater., 175 (2010) 298–303.
[3] Ö. Gerçel, H.F. Gerçel, A.S. Koparal, Ü.B. Öğütveren, Removal of disperse dye from aqueous solution by novel adsorbent prepared from biomass plant material, J. Hazard. Mater., 160 (2008) 668–674.
[4] A. Naghizadeh, M. Kamranifar, A.R. Yari, M.J. Mohammadi, Equilibrium and kinetics study of reactive dyes removal from aqueous solutions by bentonite nanoparticles, Desal. Wat. Treat., 97 (2017) 329–337.
[5] G. Zeydouni, R. Rashidi, G. Kianizadeh, Y. Omidi Khaniabadi, H. Nourmoradi, S. Esmaeili, M.J. Mohammadi, Eriochrme black-T removal from aqueous environment by surfactant modified clay: equilibrium, kinetic, isotherm, and thermodynamic studies, Toxin Rev., (2018) 1–11, http://eprints.skums.ac.ir/id/eprint/7113.
[6] H. Rezaei, M.R. Narooie, R. Khosravi, M.J. Mohammadi, H. Sharafi, H. Biglari, Humic acid removal by electrocoagulation process from natural aqueous environments, Int. J. Electrochem. Sci., 13 (2018) 2379–2389.
[7] Y.O. Khaniabadi, H. Basiri, H. Nourmoradi, M.J. Mohammadi, A.R. Yari, S. Sadeghi, A. Amrane, Adsorption of Congo Red Dye from aqueous solutions by montmorillonite as a low-cost adsorbent, Int. J. Chem. Reactor Eng., 16 (2018) 1–11.
[8] F. Salimi, H. Rahimi, C. Karami, Removal of methylene blue from water solution by modified nanogoethite by Cu, Desal. Wat. Treat., 137 (2019) 334–344.
[9] O.A. Attallah, M.A. Al-Ghobashy, M. Nebsen, M.Y. Salem, Removal of cationic and anionic dyes from aqueous solution with magnetite/pectin and magnetite/silica/pectin hybrid nanocomposites: kinetic, isotherm and mechanism analysis, RSC Adv., 6 (2016) 11461–11480.
[10] R. Si, Y.W. Zhang, L.P. You, C.H. Yan, Rare-earth oxide nanopolyhedra, nanoplates, and nanodisks, Angew. Chem. Int. Ed., 117 (2005) 3320–3324.
[11] L. Manna, D.J. Milliron, A. Meisel, E.C. Scher, A.P. Alivisatos, Controlled growth of tetrapod-branched inorganic nanocrystals, Nat. Mater., 2 (2013) 382–385.
[12] S.U. Son, I.K. Park, J. Park, T. Hyeon, Synthesis of Cu_2O coated Cu nanoparticles and their successful applications to Ullmann-type amination coupling reactions of aryl chlorides, Chem. Commun., (2004) 778–779, doi: 10.1039/B316147A.
[13] P. Malik, S. Saha, Oxidation of direct dyes with hydrogen peroxide using ferrous ion as catalyst, Sep. Purif. Technol., 31 (2003) 241–250.
[14] M. Koch, A. Yediler, D. Lienert, G. Insel, A. Kettrup, Ozonation of hydrolyzed azo dye reactive yellow 84 (CI), Chemosphere, 46 (2002) 109–113.
[15] T. Panswad, S. Wongchaisuwan, Mechanisms of dye wastewater colour removal by magnesium carbonate-hydrated basic, Water Sci. Technol., 18 (1986) 139–144.

[16] G. Ciardelli, L. Corsi, M. Marcucci, Membrane separation for wastewater reuse in the textile industry, Resour. Conserv. Recycl., 31 (2001) 189–197.
[17] N. Thinakaran, P. Baskaralingam, M. Pulikesi, P. Panneerselvam, S. Sivanesan, Removal of Acid Violet 17 from aqueous solutions by adsorption onto activated carbon prepared from sunflower seed hull, J. Hazard. Mater., 151 (2008) 316–322.
[18] M. Anbia, S.E. Moradi, Adsorption of naphthalene-derived compounds from water by chemically oxidized nanoporous carbon, Chem. Eng. J., 148 (2009) 452–458.
[19] M. Anbia, K. Mohammadi, Novel and efficient nanoporous adsorbent for dichromate ion and furfural removal from aqueous solutions, Asian J. Chem., 21 (2009) 3347–3354.
[20] A. Namane, A. Mekarzia, K. Benrachedi, N. Belhaneche-Bensemra, A. Hellal, Determination of the adsorption capacity of activated carbon made from coffee grounds by chemical activation with $ZnCl_2$ and H_3PO_4, J. Hazard. Mater., 119 (2005) 189–194.
[21] D. Aman, T. Zaki, S. Mikhail, S.A. Selim, Synthesis of a perovskite $LaNiO_3$ nanocatalyst at a low temperature using single reverse microemulsion, Catal. Today, 164 (2011) 209–213.
[22] A.L.A. Marinho, R.C. Rabelo-Neto, F.B. Noronha, L.V. Mattos, Steam reforming of ethanol over Ni-based catalysts obtained from $LaNiO_3$ and $LaNiO_3/CeSiO_2$ perovskite-type oxides for the production of hydrogen, Appl. Catal., A, 520 (2016) 53–64.
[23] A. Jahangiri, M. Saidi, F. Salimi, A. Mohammadi, Combined methane reforming over nano $LaNiO_3$ catalyst with modified active surface, Res. Chem. Intermed., 44 (2018) 1755–1773.
[24] Y. Li, S. Yao, W. Wen, L. Xue, Y. Yan, Sol–gel combustion synthesis and visible-light-driven photocatalytic property of perovskite $LaNiO_3$, J. Alloys Compd., 491 (2010) 560–564.
[25] W. Zhong, T. Jiang, Y. Dang, J. He, S.-Y. Chen, C.-H. Kuo, D. Kriz, Y. Meng, A.G. Meguerdichian, S.L. Suib, Mechanism studies on methyl orange dye degradation by perovskite-type $LaNiO_3$-δ under dark ambient conditions, Appl. Catal., A, 549 (2018) 302–309.
[26] J.-M. Wu, W. Wen, Catalyzed degradation of azo dyes under ambient conditions, Environ. Sci. Technol., 44 (2010) 9123–9127.
[27] O.P. Taran, A.B. Ayusheev, O.L. Ogorodnikova, I.P. Prosvirin, L.A. Isupova, V.N. Parmon, Perovskite-like catalysts $LaBO_3$ (B=Cu, Fe, Mn, Co, Ni) for wet peroxide oxidation of phenol, Appl. Catal., B, 180 (2016) 86–93.
[28] K.-Y.A. Lin, Y.-C. Chen, Y.-F. Lin, $LaMO_3$ perovskites (M=Co, Cu, Fe and Ni) as heterogeneous catalysts for activating peroxymonosulfate in water, Chem. Eng. Sci., 160 (2017) 96–105.
[29] B. Palas, G. Ersöz, S. Atalay, Catalytic wet air oxidation of Reactive Black 5 in the presence of $LaNiO_3$ perovskite catalyst as a green process for azo dye removal, Chemosphere, 209 (2018) 823–830.
[30] F. Salimi, M. Abdollahifar, P. Jafari, M. Hidaryan, A new approach to synthesis and growth of nanocrystalline AlOOH with high pore volume, J. Serb. Chem. Soc., 82 (2017) 203–213.
[31] F. Salimi, M. Abdollahifar, A.R. Karami, The effect of NaOH and KOH on the characterization of mesoporous AlOOH in the Solvothermal route, Ceramics–Silikáty, 60 (2016) 273–277.
[32] F. Salimi, S.S. Emami, C. Karami, Removal of methylene blue from water solution by modified nano-boehmite with Bismuth, Inorg. Nano-Met. Chem., 48 (2018) 31–40.
[33] F. Salimi, M. Eskandari, C. Karami, Investigating of the methylene blue adsorption of wastewater using modified nano-zeolite by copper, Desal. Wat. Treat., 85 (2017) 206–214.
[34] F. Salimi, K. Tahmasobi, C. Karami, A. Jahangiri, Preparation of modified nano-SiO_2 by bismuth and iron as a novel remover of methylene blue from water solution, J. Mexican Chem. Soc., 61 (2017) 250–259.
[35] M. Mohamadi, F. Salimi, S. Sadeghi, Reduction of oil, COD and turbidity of Kermanshah oil refinery effluent using modified nano-zeolite by bismuth and iron, Desal. Wat. Treat., 97 (2017) 151–157.
[36] M. Goldwasser, M.E. Rivas, E. Pietri, M. Pérez-Zurita, M. Cubeiro, A. Grivobal-Constant, G. Leclercq, Perovskites as catalysts precursors: synthesis and characterization, J. Mol. Catal. A: Chem., 228 (2005) 325–331.
[37] L. Predoana, B. Malic, M. Kosec, M. Carata, M. Caldararu, M. Zaharescu, Characterization of $LaCoO_3$ powders obtained by water-based sol–gel method with citric acid, J. Eur. Ceram. Soc., 27 (2007) 4407–4411.
[38] J. Shu, S. Kaliaguine, Well-dispersed perovskite-type oxidation catalysts, Appl. Catal., B, 16 (1998) L303–L308.
[39] L. Cui, Y. Wang, L. Gao, L. Hu, L. Yan, Q. Wei, B. Du, EDTA functionalized magnetic graphene oxide for removal of Pb(II), Hg(II) and Cu(II) in water treatment: Adsorption mechanism and separation property, Chem. Eng. J., 281 (2015) 1–10.
[40] X. Deng, L. Lü, H. Li, F. Luo, The adsorption properties of Pb(II) and Cd(II) on functionalized graphene prepared by electrolysis method, J. Hazard. Mater., 183 (2010) 923–930.
[41] R. Leyva-Ramos, L. Bernal-Jacome, I. Acosta-Rodriguez, Adsorption of cadmium (II) from aqueous solution on natural and oxidized corncob, Sep. Purif. Technol., 45 (2005) 41–49.
[42] C. Moreno-Castilla, M. Lopez-Ramon, F. Carrasco-Marın, Changes in surface chemistry of activated carbons by wet oxidation, Carbon, 38 (2000) 1995–2001.
[43] Y. Liu, X. Li, Z. Xu, Z. Hu, Preparation of flower-like and rod-like boehmite via a hydrothermal route in a buffer solution, J. Phys. Chem. Solids, 71 (2010) 206–209.
[44] S.Z. Ali, M. Athar, M. Salman, M.I. Din, Simultaneous removal of Pb(II), Cd(II) and Cu(II) from aqueous solutions by adsorption on *Triticum aestivum*-a green approach, Hydrol.: Curr. Res., 2 (2011) 118–128.
[45] J.-Z. Guo, B. Li, L. Liu, K. Lv, Removal of methylene blue from aqueous solutions by chemically modified bamboo, Chemosphere, 111 (2014) 231–225.
[46] A. Modwi, L. Khezami, K. Taha, O. Al-Duaij, A. Houas, Fast and high efficiency adsorption of Pb(II) ions by Cu/ZnO composite, Mater. Lett., 195 (2017) 41–44.
[47] L. Khezami, K.K. Taha, M. OuldM›hamed, O. Lemine, (x)ZnO(1−x) Fe_2O_3 nanocrystallines for the removal of cadmium(II) and nickel(II) from water: kinetic and adsorption studies, J. Water Supply Res. Technol. AQUA, 66 (2017) 381–391.
[48] G. Moradi, M. Rahmanzadeh, The influence of partial substitution of alkaline earth with La in the $LaNiO_3$ perovskite catalyst, Catal. Commun., 26 (2012) 169–172.
[49] R. Pereñíguez, V.M. González-DelaCruz, J.P. Holgado, A. Caballero, Synthesis and characterization of a $LaNiO_3$ perovskite as precursor for methane reforming reactions catalysts, Appl. Catal., B, 93 (2010) 346–353.
[50] M. Goldwasser, V. Dorantes, M. Pérez-Zurita, P. Sojo, M. Cubeiro, E. Pietri, F. González-Jiménez, Y.N. Lee, D. Moronta, Modified iron perovskites as catalysts precursors for the conversion of syngas to low molecular weight alkenes, J. Mol. Catal. A: Chem., 193 (2003) 227–236.
[51] M. Heidari-Chaleshtori, A. Nezamzadeh-Ejhieh, Clinoptilolite nano-particles modified with aspartic acid for removal of Cu(II) from aqueous solutions: isotherms and kinetic aspects, New J. Chem., 39 (2015) 9396–9406.
[52] M. Kosmulski, pH-dependent surface charging and points of zero charge II. Update, J. Colloid Interface Sci., 275 (2004) 214–224.
[53] J. Rezaee, F. Salimi, C. Karami, Removal of Eriochrome Black T dye from water solution using modified nano-boehmite by organic compounds, Desal. Wat. Treat., 139 (2019) 342–351.
[54] T. Madrakian, A. Afkhami, M. Ahmadi, Adsorption and kinetic studies of seven different organic dyes onto magnetite nanoparticles loaded tea waste and removal of them from wastewater samples, Spectrochim. Acta, Part A, 99 (2012) 102–109.
[55] B.S. Inbaraj, J. Wang, J. Lu, F. Siao, B. Chen, Adsorption of toxic mercury (II) by an extracellular biopolymer poly (γ-glutamic acid), Bioresour. Technol., 100 (2009) 200–207.
[56] V.S. Mane, I.D. Mall, V.C. Srivastava, Kinetic and equilibrium isotherm studies for the adsorptive removal of Brilliant Green dye from aqueous solution by rice husk ash, J. Environ. Manage., 84 (2007) 390–400.
[57] P. Pimentel, M. Melo, D. Melo, A. Assuncao, D. Henrique, C. Silva, G. Gonzalez, Kinetics and thermodynamics of Cu(II)

adsorption on oil shale wastes, Fuel Process. Technol., 89 (2008) 62–67.
[58] G. Sheng, J. Li, D. Shao, J. Hu, C. Chen, Y. Chen, X. Wang, Adsorption of copper (II) on multiwalled carbon nanotubes in the absence and presence of humic or fulvic acids, J. Hazard. Mater., 178 (2010) 333–340.
[59] G. McKay, Use of Adsorbents for the Removal of Pollutants From Wastewater, CRC Press, Boca Raton, Florida, United States, 1995.
[60] J. Wang, S. Dong, C. Yu, X. Han, J. Guo, J. Sun, An efficient MoO_3 catalyst for in-practical degradation of dye wastewater under room conditions, Catal. Commun., 92 (2017) 100–104.
[61] L. Hua, H. Ma, L. Zhang, Degradation process analysis of the azo dyes by catalytic wet air oxidation with catalyst CuO/γ-Al_2O_3, Chemosphere, 90 (2013) 143–149.
[62] G. Ovejero, A. Rodríguez, A. Vallet, J. García, Catalytic wet air oxidation of a non-azo dye with Ni/MgAlO catalyst, Chem. Eng. J., 215 (2013) 168–173.
[63] L. Zou, Q. Wang, Z. Wang, L. Jin, R. Liu, X. Shen, Rapid decolorization of methyl blue in aqueous solution by recyclable microchannel-like $La_{0.8}K_{0.2}FeO_3$ hollow microfibers, Ind. Eng. Chem. Res., 53 (2013) 658–663.
[64] Y. Xu, X. Li, X. Cheng, D. Sun, X. Wang, Degradation of cationic red GTL by catalytic wet air oxidation over Mo–Zn–Al–O catalyst under room temperature and atmospheric pressure, Environ. Sci. Technol., 46 (2012) 2856–2863.